Front. Mater. Sci. 2024, 18(4): 240703
https://doi.org/10.1007/s11706-024-0703-y

RESEARCH ARTICLE

The antibacterial and drug-loaded bilayer poly(ε-caprolactone) fibrous membrane with a shish-kebab structure

Chang Mao, Shan Liang, Yinchun Hu (✉), Yan Wei, and Di Huang

Research Center for Nano-Biomaterials & Regenerative Medicine, Department of Biomedical Engineering, College of Biomedical Engineering, Taiyuan University of Technology, Taiyuan 030024, China

ABSTRACT: Electrospinning has been widely used in the field of biomedical materials characterized with high porosity and good breathability as well as similarity to the natural extracellular matrix. This study employs the microsol-electrospinning technology combined with the self-induced crystallization method to fabricate the functionalized bilayer poly(ε-caprolactone) (PCL) fibrous membrane with a shish-kebab (SK) structure. The outer layer consists of the antibacterial SK-structured fibrous membrane showing favorable mechanical properties and notable inhibitory effects on the growth of *E. coli* and *S. aureus*, while salvianic acid A sodium (SAS) is encapsulated in the inner core–shell and SK-structured PCL fibrous membrane, achieving the controlled and sustained release of SAS. Moreover, good biocompatibility and enhanced cell adhesion of this membrane are also revealed. This antibacterial and drug-loaded bilayer PCL fibrous membrane with a SK structure demonstrates superior mechanical characteristics, exceptional antibacterial properties, and notable biocompatibility, suggesting its favorable outlook for future development in the area of tissue engineering.

KEYWORDS: poly(ε-caprolactone); salvianic acid A sodium; electrospinning; shish-kebab

Contents

Received July 2, 2024; accepted October 3, 2024

E-mail: huyinchun@tyut.edu.cn

1 Introduction

Electrospinning is a straightforward and adaptable method that can be employed to produce nanofibers for a wide range of polymers and composite materials [1–3]. Electrospun fibers, characterized by their high porosity and superior breathability as well as the similarity to natural extracellular matrix (ECM), have found extensive applications in areas such as wound dressings, periodontal treatment, and bone repair [3–6]. In a study conducted by Nanditha et al. [7], nanofiber mats composed of poly(lactic-co-glycolic acid) (PLGA) and collagen were fabricated via the electrospinning technique, which displayed a structure resembling ECM, promoting cell proliferation and migration, thereby favoring skin regeneration in wound healing.

Although electrospun fiber membranes have structural similarity to ECM, they do not possess the micro/nano-topography found on the surfaces of natural collagen nanofibrils [8–9]. The micro/nano-topography of ECM plays a crucial role in the modulation of interactions between cells and ECM [10]. Consequently, it is necessary to create the collagen-like micro/nano-topography on electrospun nanofibrils. Self-induced crystallization is a simple and commonly used technique for the surface modification of nanofibers, involving the incubation of fibers in a dilute polymer solution that has undergone crystallization. The unbound chains in the solution undergo crystallization on the surfaces of fibers, resulting in the formation of individual crystals that exhibit periodic repetition along the fiber axis [11–13]. Hence, the fiber membrane can develop a nanoscale lamellar structure resembling that of natural collagen through the utilization of the self-induced crystallization technology [14]. Using such a technology, Guo et al. successfully decorated electrospun nanofibers with a shish-kebab (SK) structure, which facilitated cell adhesion and migration [15]. Liu et al. generated SK structures of two sizes on the fiber surfaces, to which the cellular response was notably improved [16].

In order to prevent bacterial invasion and promote tissue repair, a variety of pharmaceuticals and growth factors have been integrated into electrospun fiber membranes [17–19]. Poly(ε-caprolactone) (PCL), a frequently utilized polymer, exhibits excellent plasticity and cell compatibility [20–23]. Its slow degradation rate makes it an ideal drug carrier for long-term drug delivery systems [24–26]. *Salvia miltiorrhiza*, a well-known traditional Chinese herb, has demonstrated anti-thrombotic, oxygen free radical scavenging, and anti-apoptotic properties [27–30]. However, *Salvia miltiorrhiza* is unstable under natural conditions. Therefore, it has been converted to its sodium salt form, known as salvianic acid A sodium (SAS), which maintains the same functionality as *Salvia miltiorrhiza* [31].

Considering the factors mentioned above, we utilize the electrospinning method combined with the self-induced crystallization technology to fabricate a bilayer fibrous membrane (Fig. 1). The outer layer consists of the antibacterial zinc oxide-containing SK-structured PCL (PCLSK@ZnO) fibrous membrane, while the inner layer is composed of the SAS-containing core–shell and SK-structured PCL (MSSK-SAS) fibrous membrane. The PCLSK@ZnO fibrous membrane, coated with ZnO nanoparticles (NPs) on its surface, demonstrates

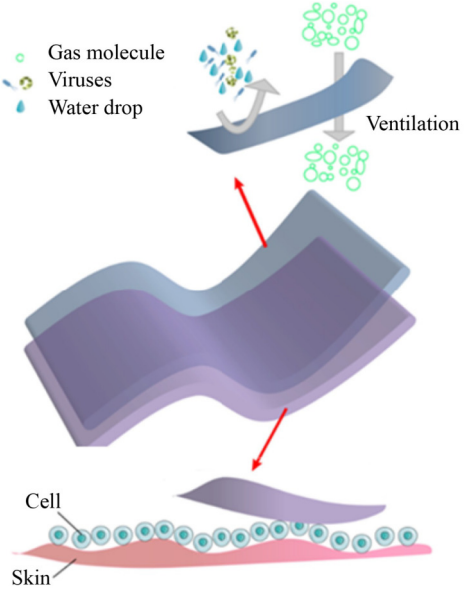

Fig. 1 Conceptual diagram illustrating the functionality of a bilayer fibrous membrane.

remarkable antibacterial effectiveness along with outstanding breathability and mechanical characteristics, while the MSSK-SAS fibrous membrane serves as a drug carrier, enabling the controlled release of SAS and exhibiting excellent cytocompatibility.

2 Experimental

2.1 Materials

PCL was purchased from Shanghai Yuanye Bio-Technology Co., Ltd. Dichloromethane (DCM), *N*,*N*-dimethylformamide (DMF), and acetic acid were purchased from Shanghai Titan Technology Co., Ltd. Nanoscale ZnO (≥ 99%) was purchased from Shanghai Macklin Biochemical Co., Ltd. SAS (≥ 99%) was purchased from Xi'an Hongsheng Biotechnology Co., Ltd. Sodium hyaluronate (SH; 95%) was purchased from Shanghai Aladdin Biochemical Technology Co., Ltd. The Cell Counting Kit-8 (CCK-8) assay kit, Calcein/PI staining kit, dimethyl sulfoxide (DMSO), penicillin–streptomycin solution, Western and IP cell lysis buffer, Trypsin-EDTA cell digestion solution, fetal bovine serum (FBS), and high-glucose Dulbecco's modified Eagle's medium (DMEM) culture medium were purchased from Shanghai Biyunet Biotechnology Co., Ltd.

2.2 Preparation of PCLSK@ZnO fibrous membranes

PCL was added into a spinning solution prepared via stirring a mixture of DCM and DMF with the volume ratio of 7:3, resulting in the formation of a PCL electrospinning solution with the mass fraction of 18%. The electrospinning process was then carried out at room temperature under the following conditions: a spinning voltage of 18 kV, a collecting distance of 15 cm, a flow rate of 0.003 mm·s^{-1}, and a drum rotation speed of 350 r·min^{-1}. A 1% PCL in acetic acid solution was prepared using 75% acetic acid. Subsequently, PCL nanofiber membranes were immersed in the PCL solution at room temperature for 5, 10, 15, 20, 30, 60, 90, and 120 min, and the obtained samples were denoted as PCLSK5, PCLSK10, PCLSK15, PCLSK20, PCLSK30, PCLSK60, PCLSK90, and PCLSK120, respectively. After washing with distilled water followed by drying, such PCLSK fibrous membranes were loaded with a 2% aqueous solution of ZnO NPs to obtain them.

2.3 Preparation of MSSK-SAS fibrous membranes

A mixture of SH (1 wt.%) and SAS (100 μL·mL^{-1}) was prepared through mixing their water-soluble solutions. The oil-in-water (O/W) emulsion containing uniformly micronized particles was prepared by adding sorbitan monooleate (SMO), which acted as an emulsifier, and DCM into the mixture of SH and SAS followed by high-speed stirring. PCL and DMF were then dissolved in the emulsion to obtain the micro-solvated electrospinning solution. Afterwards, electrospinning was performed under the conditions with a spinning voltage of 18 kV, a receiving distance of 15 cm, a flow rate of 0.001 mm·s^{-1}, and a drum rotation speed of 350 r·min^{-1}. Subsequently a 1 wt.% solution of PCL in acetic acid was stirred magnetically at 60 °C for 1 h followed by cooling to room temperature. After approximately 30 μL of the solution was slowly dropped onto a PCL fibrous membrane with different durations of 0, 5, 10, 15, 20, and 30 min for droplet deposition, samples were washed with deionized water and dried in an oven for the evaporation of the solvent, resulting in the formation of PCL spherulite structures. Such samples were denoted as MS-SAS, MSSK5-SAS, MSSK10-SAS, MSSK15-SAS, MSSK20-SAS, and MSSK30-SAS, respectively, according to their different durations of time for self-induced crystallization. The preparation process of core−shell and SK-structured PCL (MSSK) fibrous membranes is the same as that of MSSK-SAS fibrous membranes except for the replacement of the mixed solution between SH and SAS with the SH aqueous solution.

2.4 Material characterizations

Ultraviolet–visible (UV–Vis) spectrophotometry was carried out to record UV and visible spectra of tested samples. The surface morphology of samples was detected through scanning electron microscopy (SEM) conducted on a JMF-7100F microscope. Fourier transform infrared spectroscopy (FTIR) was performed using an Alpha II instrument. Tensile properties of the fibrous membrane were tested using a REGER RGM-05 instrument. Cell proliferation results were obtained through the measurement of absorbance values based on the optical density (OD) using an enzyme-linked immunosorbent assay (ELISA) reader. The cellular status (vitality) was evaluated via inverted fluorescence microscopy (IFM).

2.5 Antibacterial properties

To evaluate antibacterial properties of any fibrous membrane, Gram-positive *Staphylococcus aureus* (*S. aureus*) and Gram-negative *Escherichia coli* (*E. coli*) were selected for testing, and the antibacterial effects were evaluated using the inhibition zone method. After *E. coli* and *S. aureus* were separately cultured in the shaking incubator at 37 °C for approximately 24 h, the obtained bacterial suspension was diluted, 100 μL of which was then uniformly spread on the agar medium. Afterwards, the fibrous membrane was placed on the solid agar medium and cultured at (37 ± 0.5) °C for 24 h. The diameters of inhibition zones around samples were finally acquired, each of which was measured three times for repeatability.

2.6 Drug release

The dried MSSK20-SAS fibrous membrane was placed in a test tube containing 10 mL of phosphate-buffered saline (PBS) at pH 7.4. The test tube was then subjected to constant-temperature oscillation at 37 °C. At regular intervals, the solution from the test tube was withdrawn. After both the test tube and the fibrous membrane were rinsed with PBS, an equal amount of PBS was added back to maintain a constant volume. The absorbance of the solution was measured using a UV–Vis spectrophotometer at the maximum absorption wavelength (λ = 280 nm) of SAS [27]. The amount of drug released from the nanofiber membrane during a specific period of time was calculated based on the drug standard curve equation, and cumulative data were adopted to generate the release profile.

2.7 Characterization of biocompatibility

2.7.1 Cell culture

Before culturing, samples were sliced into discs 1 cm in diameter, sterilized with a 75% ethanol solution, subjected to overnight UV light exposure, washed with PBS, and subsequently transferred into a 24-well culture plate. Human skin fibroblasts (HSFs) were chosen and seeded onto each fiber membrane in a 24-well plate at a density of 5 × 10^3 cells/well, with the fresh complete medium replaced every 24 h. Seed HSFs utilized in this study were obtained from the Shanghai Cell Bank which is part of the Chinese Academy of Sciences (CAS).

2.7.2 Cell proliferation

Fibrous membranes were co-cultured with cells for durations of 1, 3, and 5 d, separately. A CCK-8 reagent was prepared at a volume ratio of 1:19 between CCK-8 and DMEM, with 700 μL of the CCK-8 reagent added to each well, and then it was incubated in the dark for 2 h, followed by transferring 100 μL of the CCK-8 solution to a 96-well plate. The absorbance of the detection liquid at 450 nm was measured using an ELISA reader to evaluate cell proliferation.

2.7.3 Cell viability assay

The 24-well plates, containing cells cultured separately for 1, 3, and 5 d, were subjected to the Calcein/PI Cell Viability and Cytotoxicity Assay Kit, incubated at 37 °C for 30 min, and then washed to observe and capture the live/dead status of the cells with IFM.

2.7.4 Cell adhesion

Human fibroblast cells were seeded onto the fibrous membrane in each well of a 24-well plate at a density of 5 × 10^3 cells/well followed by culturing for 5 d with the culture medium replaced every 24 h. Subsequently, samples were fixed with 2% glutaraldehyde at room temperature for 2 h. After dehydration using an ethanol gradient (30%, 50%, 75%, 85%, 95%, 100%), samples were coated with metal in vacuum, facilitating the observation of surface morphology and the measurement of cell adhesion through SEM.

2.8 Statistical analysis

Experimental data in this study were obtained from three parallel samples, and the results were presented as mean ± standard deviation (SD). Statistical significance was evaluated using one-way analysis of variance (ANOVA), and a p value less than 0.05 was considered to indicate a significant difference (*p < 0.05, **p < 0.01, ***p < 0.001).

3 Results and discussion

3.1 Microstructures and mechanical properties of PCLSK fibrous membranes

Surface morphologies of different PCLSK fibrous

membranes were observed through SEM. As shown in Fig. 2, it was revealed that the hydrophobic PCL electrospun nanofibers did not exhibit significant breaks, and the fibers appeared relatively straight with a uniform distribution. The average fiber diameter ranged from 100 to 300 nm. After the self-induced crystallization of PCL nanofibers, a periodic arrangement of two-dimensional (2D) "disk-shaped" PCL crystal lamellae perpendicular to the nanofiber axis was observed on the fiber surface. To investigate the effect of different induction crystallization time periods on the fiber structure, Figs. 2(b)–2(g) demonstrate changes in the surface morphology and crystal size with varying induction crystallization time periods, illustrating the morphological characteristics of the crystal lamellae attached to the PCL fibrous membrane corresponding to different time periods for culturing. Compared to fibers before self-induced crystallization, diameter of PCL nanofibers is smaller. After immersion for 10 min in self-induced crystallization, a crystal lamellar layer forms on the surface of the PCL nanofibers. These lamellae are extremely small and only slightly protrude. With prolonging the immersion time, the crystal lamellar layer grows, and completely encloses the fibers. When the culture time reaches 120 min, the crystal lamellar layer collapses, and adjacent lamellae merge with each other. At this point, periodicity increases to 1169 nm. With the prolonging of crystallization time, lamellae continue to

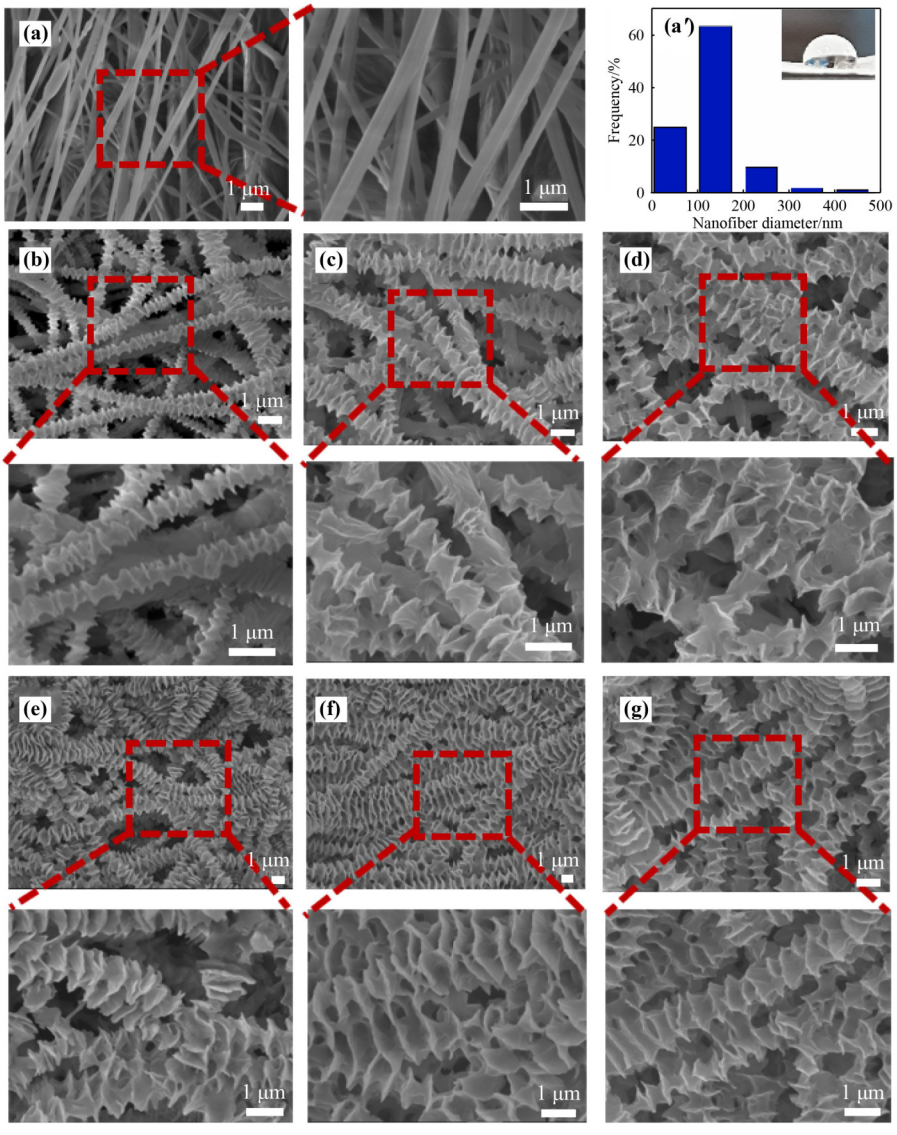

Fig. 2 SEM images of outer-layer PCLSK fibrous membranes: (**a**) PCL ((**a′**) PCL fiber diameter distribution); (**b**) PCLSK10; (**c**) PCLSK20; (**d**) PCLSK35; (**e**) PCLSK60; (**f**) PCLSK90; (**g**) PCLSK120.

grow, and irregular lamellar morphologies could be observed. This might be due to the merging and continued growth of adjacent lamellae from different directions when they meet, ultimately resulting in the formation of the irregular coral-like surface structure. Another possibility is that when the fibrous membrane is immersed in a diluted PCL solution, the orientation of PCL nanofibers is limited, and molecular chains in solution aggregate onto nanofibers at different angles. With prolonging the self-induced crystallization time, a large number of lamellae compete for growth within a limited space, leading to the distorted lamellar growth.

According to FTIR spectra of PCL and PCLSK120@ZnO fibrous membranes shown in Fig. 3(a), their strong absorption peak positions and numbers are very similar, indicating that the fibrous membranes only suffered from a morphological change during the loading process of ZnO, and the molecular structure did not undergo significant changes. The stretching vibration peak of the C−H bond is located at 2921 cm^{-1}, while the absorption peak corresponding to the stretching vibration of ester bond (C=O) is located at 1707 cm^{-1}. Such two characteristic peaks are associated with the presence of PCL [32]. The peak at 412 cm^{-1} should be attributed to the Zn−O vibration [33]. Combined with the SEM image and the energy dispersive spectroscopy (EDS) Zn mapping image of the PCLSK120@ZnO fibrous membrane shown in Fig. 3(b), it could be deduced that ZnO had been successfully loaded onto the fibrous membrane.

Given the influence of self-induced crystallization on the microstructure and fiber diameter, experiments were carried out to investigate tensile properties of fibrous membranes with different self-induced crystallization periods of time. As depicted in Fig. 4, the tensile strength and elastic modulus of the PCLSK120 fibrous membrane with self-induced crystallization exhibited significantly higher values compared to those of the PCL fibrous membrane without crystallization. Moreover, the Young's modulus of PCLSK120 showed a 203.5% improvement over that of PCL. The breaking elongation of fibrous membranes initially increased and then decreased with prolonging the soaking time, but remained slightly higher than that of the un-crystallized PCL fibrous membrane.

3.2 Antibacterial property assay of outer-layer PCL-based fibrous membranes

In order to promote wound healing and prevent bacterial infections on wound surfaces, dressings should possess certain antibacterial properties. ZnO NPs are often chosen as antimicrobial agents due to their advantages such as low cost and low toxicity [34–36]. Li et al. [37]

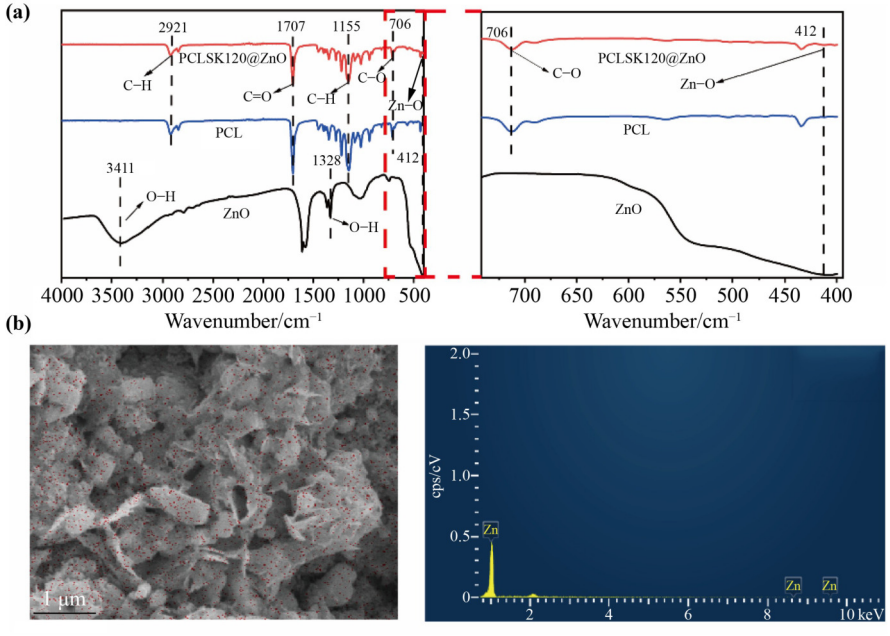

Fig. 3 (**a**) FTIR spectra of ZnO, PCL, and PCLSK120@ZnO. (**b**) SEM and EDS Zn mapping images of the PCLSK120@ZnO fibrous membrane.

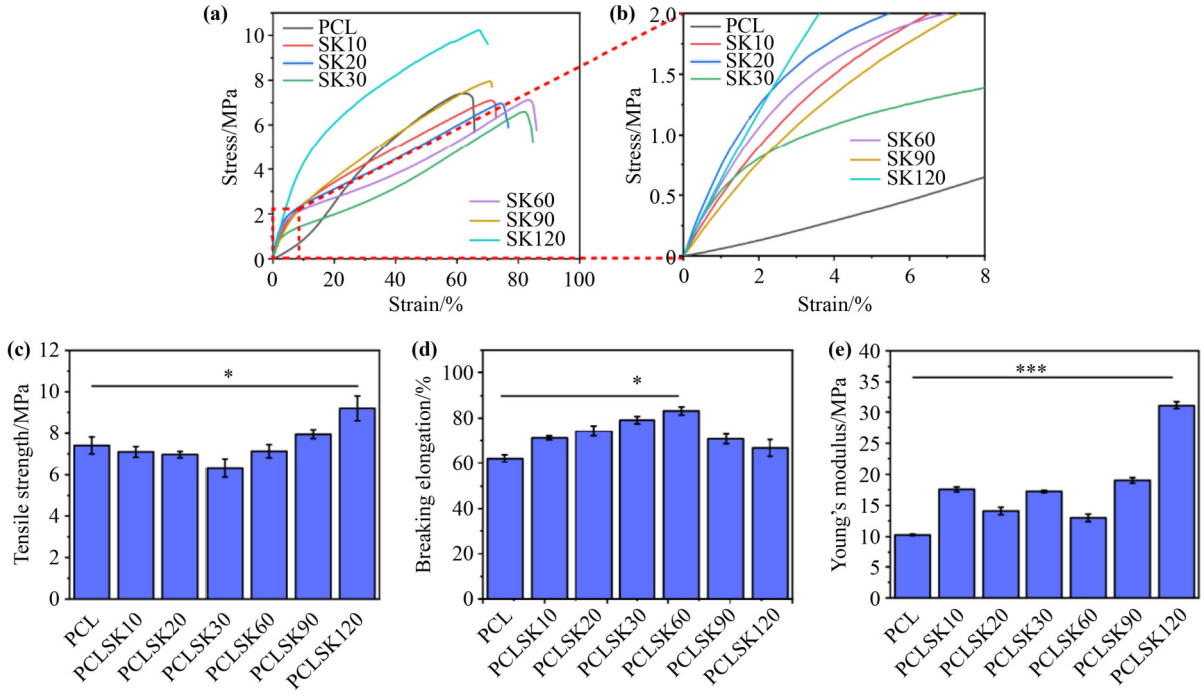

Fig. 4 Tensile properties of PCL and SK-structured PCL fibrous membranes: (**a**)(**b**) relationship between stress and strain; (**c**) tensile strength (*$p < 0.05$); (**d**) breaking elongation (*$p < 0.05$); (**e**) Young's modulus (***$p < 0.001$).

investigated the toxicity differences of nano-ZnO, analytical grade ZnO, and Zn^{2+} on *E. coli* under co-cultivation conditions in ultrapure water. The results revealed that the toxicity of nano-ZnO to bacteria mainly originates from the release of Zn^{2+}. Released Zn^{2+} from ZnO disrupts bacterial cell wall proteins, thereby achieving inhibitory effects. The antibacterial performance of fibrous membranes was evaluated using the agar diffusion method. Results of the inhibition zone experiments for *E. coli* and *S. aureus* on PCL, PCL@ZnO, and PCLSK120@ZnO fibrous membranes are shown in Fig. 5. Results indicate that the PCL material itself has limited antibacterial capability, while both PCL@ZnO and PCLSK120@ZnO fibrous membranes exhibit significant inhibition zones against *E. coli* and *S. aureus*, demonstrating good antibacterial properties. Hasannasab et al. prepared silk fibroin fibers loaded with ZnO, which exhibited significant antibacterial effects against both *E. coli* and *S. aureus*, blocking bacterial invasion and providing a favorable environment for wound healing [38]. The PCLSK120@ZnO fibrous membrane successfully loaded with ZnO effectively inhibited the proliferation of both *E. coli* and *S. aureus*, creating a sterile environment and providing favorable conditions for the subsequent treatment.

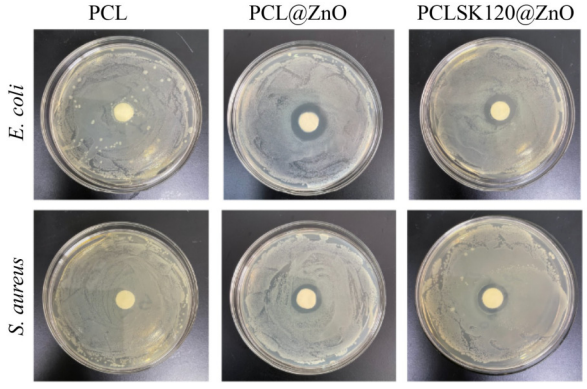

Fig. 5 Results of inhibition experiments on PCL, PCL@ZnO, and PCLSK120@ZnO fibrous membranes.

3.3 Microscopic morphology of MSSK fibrous membranes

Utilizing the micro-emulsion electrospinning technique, MS-SAS fibrous membranes were fabricated and further modified via self-induced crystallization to induce the homogeneous PCL crystallization into a spherulitic structure, resulting in the formation of the MSSK-SAS fibrous membrane. As shown in Fig. 6, SEM images reveal microstructures of fibrous membranes with different immersion time periods. After electrospinning, continuous and smooth nanofibers were obtained

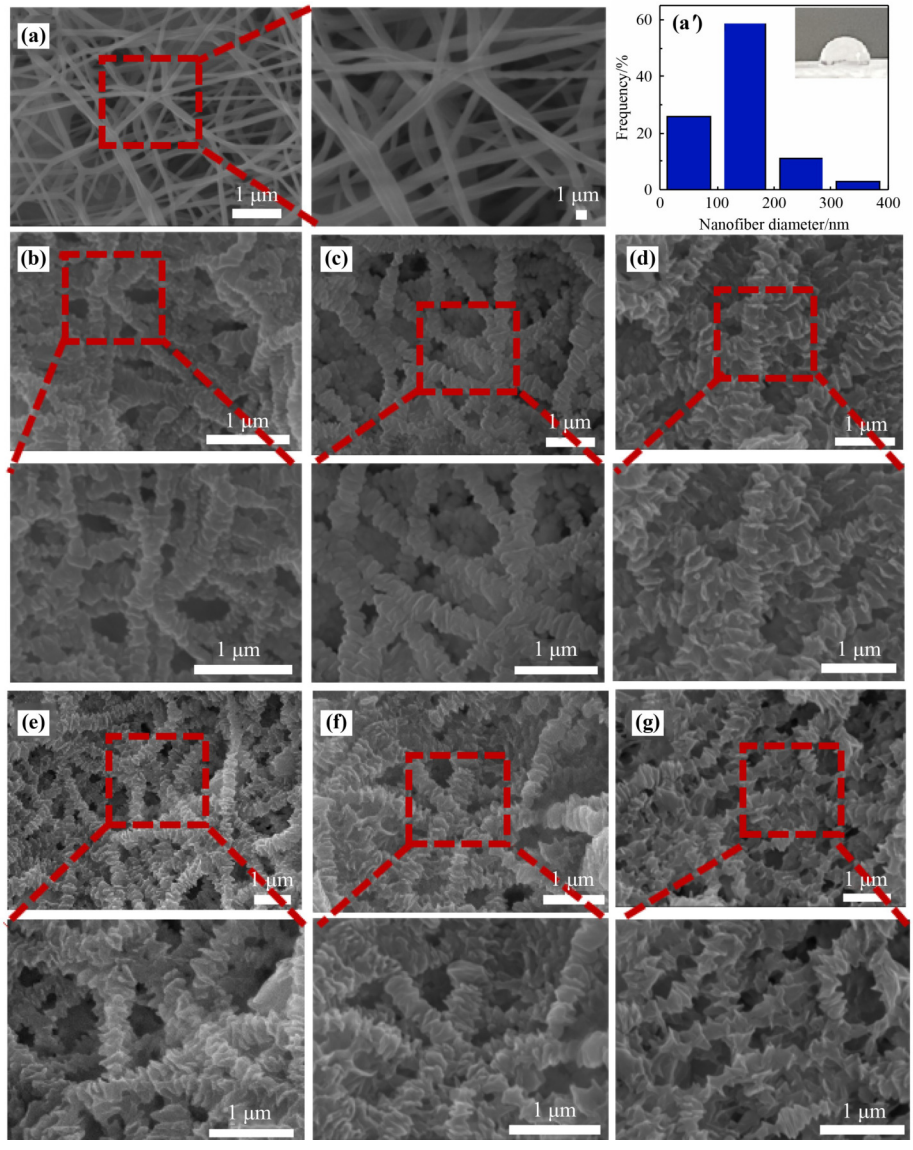

Fig. 6 SEM images of inner-layer fibrous membranes: (**a**) MS ((**a′**) PCL fiber diameter distribution); (**b**) MSSK5; (**c**) MSSK10; (**d**) MSSK15; (**e**) MSSK20; (**f**) MSSK25; (**g**) MSSK30.

(Fig. 6(a)), with a diameter of 50–300 nm suitable for the growth of HSFs. When the diluted PCL solution was dropped onto the surface of the core–shell-structured PCL (MS) fibrous membrane, the MSSK fibrous membrane with a spherulitic structure was obtained (Figs. 6(b)–6(g)), displaying morphologies of PCL crystal lamellae attached to the PCL fibrous membrane corresponding to different culture periods of time. When the culture time period was 5 min, small PCL crystal lamellae appeared on the fiber surface (Fig. 6(b)), which were tiny and only slightly protruded. With prolonging the crystallization time, lamellae continued to grow. After culturing for 30 min, such crystal lamellae collapsed, and adjacent lamellar layers merged with each other, resulting in the increase of periodicity reaching 200 nm.

3.4 Drug release of MSSK-SAS fibrous membranes

Drug release performance plays a crucial role in drug carrier materials [39–41]. The release curve of SAS serves as a significant indicator for evaluating the drug release performance of the prepared MSSK-SAS fibrous membrane. A standard curve of SAS is depicted in Fig. 7(a). To simulate physiological conditions, a drug release experiment was conducted in the PBS environment at 37 °C. As shown in Fig. 7(b), SAS exhibits a characteristic pattern of the initial rapid release followed by the sustained slow release. Specifically, the

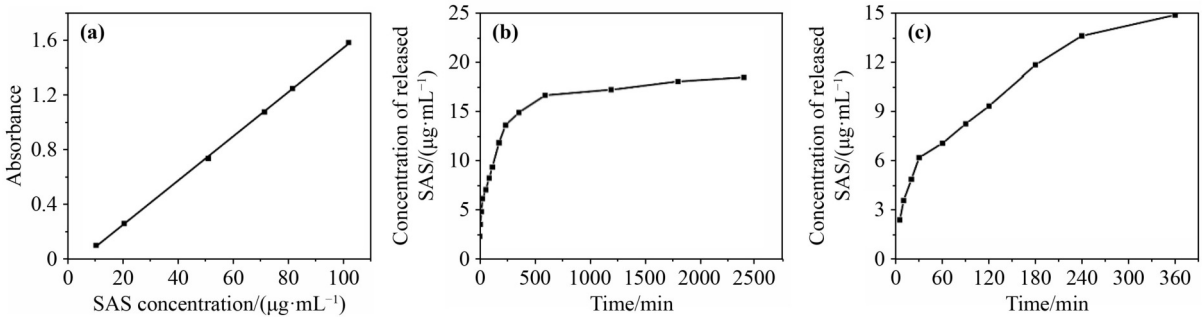

Fig. 7 Drug release characteristics: (**a**) a standard drug release curve for the SAS membrane; (**b**) a drug release curve for the MSSK-SAS fibrous membrane; (**c**) magnification of the curve corresponding to the range of 0–360 min in Panel (b).

majority of SAS was rapidly released within the first period of 6 h followed by the gradual and slow release of the remaining SAS in the fibrous membrane, eventually reaching a dynamic equilibrium of the drug concentration.

3.5 Biocompatibility evaluation of inner-layer fibrous membranes

In order to assess the biocompatibility of fibrous membranes and the influence of SAS, HSFs were co-cultured with various types of fibrous membranes, revealing the difference in viability of those cultured cells. As shown in Fig. 8(a), the density of HSFs on the surface of the fibrous membrane increased continuously with the duration of treatment. After cultivation for either 3 or 5 d, the cell density of HSFs on the fibrous membrane was significantly higher than that on the first day, merely accompanied with a small number of dead cells. Furthermore, the cell densities of MSSK-SAS and MS-SAS groups were larger than those of MS and MSSK groups, indicating a positive effect derived from the addition of SAS on the growth of HSFs.

In order to comprehensively study the biological performance of fibrous membranes in this work, a CCK-8 assay was conducted to quantitatively evaluate the impact of different fibrous membranes on the proliferation of HSFs. The results shown in Fig. 8(b) demonstrate that the absorbance values of cells in each group gradually increase with prolonging the incubation time, indicating that fibrous membranes have no inhibitory effect on the cell proliferation. This result is consistent with the findings of the live/dead cell staining. After co-incubation for 1 d, the proliferation of cells in the MSSK-SAS group was significantly higher than that in MS and MSSK groups, with statistically significant difference. Furthermore, after co-incubation for 3 d, absorbance values of cells in all groups significantly increased, and after 5 d of incubation, absorbance values in all groups more than doubled compared to Day 1. Additionally, after co-incubation for either 3 or 5 d, the absorbance value of the MSSK-SAS group was significantly higher than those of MS and MSSK groups. Fiber membranes featuring a SK structure (i.e., MSSK and MSSK-SAS) demonstrate elevated absorbance values in comparison to their counterparts in the absence of the SK structure (i.e., MS and MS-SAS). The result reveals that the presence of SAS and the possessed structure of SK can promote the proliferation of cells, which is also consistent with that from live/dead cell staining.

According to the research findings, the adhesion of a large number of cells is crucial for wound healing [42]. Therefore, we further conducted cell adhesion experiments and observed the adhesion of HSFs on the fibrous membrane through SEM. As depicted in Fig. 8(c), there were a large number of HSFs firmly attached to sample surfaces, indicating that HSFs can effectively adhere to and proliferate on the nanofiber membrane investigated in this work, conducive to the growth of new tissues. These results suggest that the prepared fibrous membrane has not toxic effect on cell growth, but good biocompatibility and improved cell adhesion properties.

4 Conclusions

This study employed solution electrospinning, self-induced crystallization, and core–shell drug loading techniques to fabricate antibacterial and drug-loaded bilayer PCL fibrous membranes with a SK structure. The outer layer, a PCLSK@ZnO fibrous membrane loaded with ZnO NPs, effectively prevents the growth of *E. coli* and *S. aureus*, thereby defending against bacterial

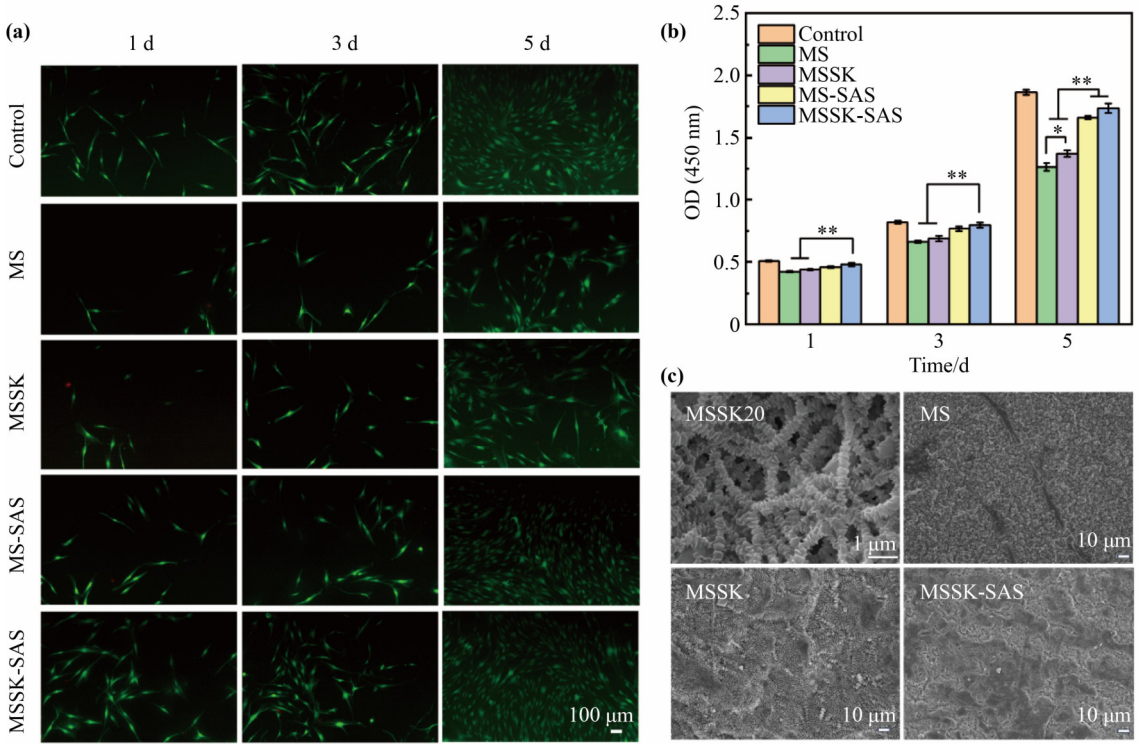

Fig. 8 Biocompatibility of inner-layer fibrous membranes: (**a**) fluorescence images of live/dead staining of fibrous membrane surfaces incubated with HSFs for 1, 3, and 5 d; (**b**) characterization of the CCK-8 proliferation on surfaces of fibrous membranes incubated with HSFs for 1, 3, and 5 d (*$p < 0.05$ and **$p < 0.01$); (**c**) SEM images showing surfaces of the MSSK20 fibrous membrane without cultured cells and MS, MSSK, and MSSK-SAS fibrous membranes with attached HSFs cultured for 5 d.

invasion. Furthermore, the PCLSK@ZnO fibrous membrane demonstrates excellent mechanical properties. Investigation into the drug release behavior of the inner layer, a MSSK-SAS fibrous membrane, verified that it can regulate the release of SAS. Cell experiments further confirmed that MSSK-SAS fibers are conducive to cell proliferation and adhesion. Therefore, we believe that this bilayer PCL fibrous membrane has great potential to be further utilized in tissue engineering applications due to its antibacterial, controlled release, and biocompatible characteristics.

Authors' contributions Chang Mao: investigation, software, and draft writing; Shan Liang: visualization, investigation, and verification; Yinchun Hu: investigation, project administration, methodology, visualization, and draft writing; Yan Wei: conceptualization and methodology; Di Huang: conceptualization, supervision, and methodology.

Declaration of competing interests The authors declare no competing financial interests.

Acknowledgements This work was supported by the General Project of Natural Science of Shanxi Province Basic Research Program (202203021211125).

References

[1] Liu H, Bai Y, Huang C, et al. Recent progress of electrospun herbal medicine nanofibers. Biomolecules, 2023, 13(1): 184

[2] Sun B, Long Y Z, Zhang H D, et al. Advances in three-dimensional nanofibrous macrostructures via electrospinning. Progress in Polymer Science, 2014, 39(5): 862−890

[3] Schulte-Werning L V, Singh B, Johannessen M, et al. Antimicrobial liposomes-in-nanofiber wound dressings prepared by a green and sustainable wire-electrospinning set-up. International Journal of Pharmaceutics, 2024, 657: 124136

[4] He J B, Zhou S S, Wang J X, et al. Anti-inflammatory and anti-oxidative electrospun nanofiber membrane promotes diabetic wound healing via macrophage modulation. Journal of Nanobiotechnology, 2024, 22(1): 116

[5] Li B, Chen Y, He J S, et al. Silk fibroin/methacrylated gelatine/hydroxyapatite biomimetic nanofibrous membranes for guided bone regeneration. International Journal of Biological Macromolecules, 2024, 263: 130380

[6] Zhou F, Cui C, Sun S, et al. Electrospun ZnO-loaded chitosan/PCL bilayer membranes with spatially designed

structure for accelerated wound healing. Carbohydrate Polymers, 2022, 282: 119131

[7] Nanditha C K, Kumar G S V. Bioactive peptides laden nano and micro-sized particles enriched ECM inspired dressing for skin regeneration in diabetic wound. Materials Today Bio, 2022, 14: 100235

[8] Fang M, Goldstein E L, Matich E K, et al. Type I collagen self-assembly: the roles of substrate and concentration. Langmuir, 2013, 29(7): 2330−2338

[9] Liu C, Jiang S, Xu W, et al. Poly-l-lactide-co-ε-caprolactone (PLCL) and poly-l-lactic acid (PLLA)/gelatin electrospun subacromial spacer improves extracellular matrix (ECM) deposition for the potential treatment of irreparable rotator cuff tears. International Journal of Biological Macromolecules, 2023, 245: 125522

[10] Bettinger C J, Langer R, Borenstein J T. Engineering substrate topography at the micro‐ and nanoscale to control cell function. Angewandte Chemie International Edition, 2009, 48(30): 5406−5415

[11] Kucinska-Lipka J, Gubanska I, Janik H, et al. Fabrication of polyurethane and polyurethane based composite fibres by the electrospinning technique for soft tissue engineering of cardiovascular system. Materials Science and Engineering C, 2015, 46: 166−176

[12] Ding H, Hu Y, Cheng Y, et al. Core–shell nanofibers with a shish-kebab structure simulating collagen fibrils for bone tissue engineering. ACS Applied Bio Materials, 2021, 4(8): 6167−6174

[13] Dai T L, Wang L N, Yao J M, et al. Self-induced crystallization to form a shish-kebab structure on PLA-based Janus membrane to promote water transmission and interlayer binding force. Separation and Purification Technology, 2024, 332: 125793

[14] Wang X, Salick M R, Wang X, et al. Poly (ε-caprolactone) nanofibers with a self-induced nanohybrid shish-kebab structure mimicking collagen fibrils. Biomacromolecules, 2013, 14(10): 3557−3569

[15] Guo X, Wang X, Li X, et al. Endothelial cell migration on poly (ε-caprolactone) nanofibers coated with a nanohybrid shish-kebab structure mimicking collagen fibrils. Biomacromolecules, 2020, 21(3): 1202−1213

[16] Liu L, Zhang T, Li C, et al. Regulating surface roughness of electrospun poly (ε-caprolactone)/β-tricalcium phosphate fibers for enhancing bone tissue regeneration. European Polymer Journal, 2021, 143: 110201

[17] He T, Wang J, Huang P, et al. Electrospinning polyvinylidene fluoride fibrous membranes containing anti-bacterial drugs used as wound dressing. Colloids and Surfaces B: Biointerfaces, 2015, 130: 278−286

[18] Zhou K, Wang M, Zhou Y, et al. Comparisons of antibacterial performances between electrospun polymer@drug nanohybrids with drug-polymer nanocomposites. Advanced Composites and Hybrid Materials, 2022, 5(2): 907−919

[19] Mottola S, Viscusi G, Belvedere R, et al. Production of mono and bilayer devices for wound dressing by coupling of electrospinning and supercritical impregnation techniques. International Journal of Pharmaceutics, 2024, 660: 124308

[20] Han J, Branford-White C J, Zhu L M. Preparation of poly (ε-caprolactone)/poly (trimethylene carbonate) blend nanofibers by electrospinning. Carbohydrate Polymers, 2010, 79(1): 214−218

[21] Wang Y, Liu Y, Qian Y, et al. Characteristics of MgO/PCL/PVP antibacterial nanofiber membranes produced by electrospinning technology. Surfaces and Interfaces, 2022, 28: 101661

[22] Chen H, Zhang J, Wu H, et al. Fabrication of a Cu nanoparticles/poly (ε-caprolactone)/gelatin fiber membrane with good antibacterial activity and mechanical property via green electrospinning. ACS Applied Bio Materials, 2021, 4(8): 6137−6147

[23] Jia X, Zhou J, Ning J, et al. The polycaprolactone/silk fibroin/carbonate hydroxyapatite electrospun scaffold promotes bone reconstruction by regulating the polarization of macrophages. Regenerative Biomaterials, 2022, 9: rbac035

[24] Malikmammadov E, Tanir T E, Kiziltay A, et al. PCL and PCL-based materials in biomedical application. Journal of Biomaterials Science: Polymer Edition, 2018, 29(7−9): 863−893

[25] Sinha V R, Bansal K, Kaushik R, et al. Poly-ε-caprolactone microspheres and nanospheres: an overview. International Journal of Pharmaceutics, 2004, 278(1): 1−23

[26] Wang X, Wang Y, Wei K, et al. Drug distribution within poly (ε-caprolactone) microspheres and *in vitro* release. Journal of Materials Processing Technology, 2009, 209(1): 348−354

[27] Liu R, Yu X, Gao W, et al. Study on the interaction between salvianic acid A sodium and bovine serum albumin by spectroscopic methods. Spectrochimica Acta Part A: Molecular and Biomolecular Spectroscopy, 2011, 78(5): 1535−1539

[28] Wang C Y, Ma F L, Liu J T, et al. Protective effect of salvianic acid A on acute liver injury induced by carbon tetrachloride in rats. Biological & Pharmaceutical Bulletin, 2007, 30(1): 44−47

[29] Chan K, Chui S H, Wong D Y L, et al. Protective effects of Danshensu from the aqueous extract of *Salvia miltiorrhiza* (Danshen) against homocysteine-induced endothelial dysfunction. Life Sciences, 2004, 75(26): 3157−3171

[30] Jia D, Zhang C R, Qiu Y, et al. Cardioprotective mechanisms of salvianic acid A sodium in rats with myocardial infarction based on proteome and transcriptome analysis. Acta Pharmacologica Sinica, 2019, 40(12): 1513−1522

[31] Jia D, Li T, Chen X, et al. Salvianic acid A sodium protects HUVEC cells against tert-butyl hydroperoxide induced oxidative

injury via mitochondria-dependent pathway. Chemico-Biological Interactions, 2018, 279: 234−242

[32] Dhandayuthapani B, Krishnan U M, Sethuraman S. Fabrication and characterization of chitosan–gelatin blend nanofibers for skin tissue engineering. Journal of Biomedical Materials Research Part B: Applied Biomaterials, 2010, 94(1): 264−272

[33] Liang H, Wang H Y, Sun X M, et al. Development of ZnO/Ag nanoparticles supported polydopamine-modified montmorillonite nanocomposites with synergistic antibacterial performance. Applied Clay Science, 2023, 244: 107112

[34] Becheri A, Dürr M, Lo Nostro P, et al. Synthesis and characterization of zinc oxide nanoparticles: application to textiles as UV-absorbers. Journal of Nanoparticle Research, 2008, 10(4): 679−689

[35] Wang X, Pan L, Zheng A, et al. Multifunctionalized carbon-fiber-reinforced polyetheretherketone implant for rapid osseointegration under infected environment. Bioactive Materials, 2023, 24: 236−250

[36] Yao L, Wu X, Wu S, et al. Atomic layer deposition of zinc oxide on microrough zirconia to enhance osteogenesis and antibiosis. Ceramics International, 2019, 45(18): 24757−24767

[37] Li M, Lin D, Zhu L. Effects of water chemistry on the dissolution of ZnO nanoparticles and their toxicity to *Escherichia coli*. Environmental Pollution, 2013, 173: 97−102

[38] Hasannasab M, Nourmohammadi J, Dehghan M M, et al. Immobilization of bromelain and ZnO nanoparticles on silk fibroin nanofibers as an antibacterial and anti-inflammatory burn dressing. International Journal of Pharmaceutics, 2021, 610: 121227

[39] Farzan M, Roth R, Schoelkopf J, et al. The processes behind drug loading and release in porous drug delivery systems. European Journal of Pharmaceutics and Biopharmaceutics, 2023, 189: 133−151

[40] Rehman F, Khan A J, Sama Z U, et al. Surface engineered mesoporous silica carriers for the controlled delivery of anticancer drug 5-fluorouracil: computational approach for the drug-carrier interactions using density functional theory. Frontiers in Pharmacology, 2023, 14: 1146562

[41] Yuan M, Liu K, Jiang T, et al. GelMA/PEGDA microneedles patch loaded with HUVECs-derived exosomes and Tazarotene promote diabetic wound healing. Journal of Nanobiotechnology, 2022, 20(1): 147

[42] Zhang H M, Guo M, Zhu T H, et al. A careob-like nanofibers with a sustained drug release profile for promoting skin wound repair and inhibiting hypertrophic scar. Composites Part B: Engineering, 2022, 236: 109790